Effect of pressure on the Cu and Pr magnetism in $Nd_{1-x}Pr_xBa_2Cu_3O_{7-\delta}$ investigated by muon spin rotation

A. Maisuradze,[1,2,*] B. Graneli,[1,3] Z. Guguchia,[1] A. Shengelaya,[4] E. Pomjakushina,[5] K. Conder,[5] and H. Keller[1]

[1]*Physik-Institut der Universität Zürich, Winterthurerstrasse 190, CH-8057 Zürich, Switzerland*
[2]*Laboratory for Muon Spin Spectroscopy, Paul Scherrer Institut, CH-5232 Villigen PSI, Switzerland*
[3]*Institute of Theoretical Physics, ETH Hönggerberg, CH-8093 Zürich, Switzerland*
[4]*Department of Physics, Tbilisi State University, Chavchavadze 3, GE-0128 Tbilisi, Georgia*
[5]*Laboratory for Developments and Methods, Paul Scherrer Institut, CH-5232 Villigen PSI, Switzerland*

The effect of pressure on the copper and praseodymium magnetic order in the system $Nd_{1-x}Pr_xBa_2Cu_3O_{7-\delta}$ with $x = 0.3$, 0.5, 0.7, and 1 was investigated by means of the muon spin rotation technique. It was found that the effect of pressure on the Néel temperatures of both copper and praseodymium is positive for the whole range of Pr concentrations ($0.3 < x < 1$) studied. These findings are in contrast with a number of previous reports and clarify some of the puzzles related to the effect of pressure on superconductivity and magnetism in the praseodymium-substituted $R_{1-x}Pr_xBa_2Cu_3O_{7-\delta}$ systems, where R is a rare-earth element.

PACS number(s): 74.72.Kf, 76.75.+i, 74.62.Fj, 75.50.Ee

I. INTRODUCTION

Substitution of rare-earth elements (R) for Y in the cuprate superconductor $YBa_2Cu_3O_{7-\delta}$ has been found not to affect the superconducting properties.[1–4] Chemically well prepared samples of $RBa_2Cu_3O_{7-\delta}$ have practically identical superconducting transition temperatures $T_c \simeq 93$ K,[4] although most of the R^{3+} elements possess a substantial magnetic moment.[5] Such behavior is explained by a weak hybridization of the R layer with the superconducting CuO_2 planes. However, there are two exceptions: Partially substituting Y with Ce and Pr substantially reduces T_c. In $R_{1-x}Pr_xBa_2Cu_3O_{7-\delta}$ superconductivity is suppressed completely for $x > x_{cr}$.[3,6–11] In the case of Ce the reason for the T_c suppression is understood as a result of its $4+$ valence state in contrast to $3+$ for most of the R elements.[3] On the other hand a large number of results obtained with different techniques point to a $3+$ valence state of Pr (see, e.g., Refs. [12–14]). Thus, Pr is the exceptional three-valent rare-earth element which substantially influences the superconducting and magnetic properties of $R_{1-x}Pr_xBa_2Cu_3O_{7-\delta}$.[10,15] Moreover, for a rare-earth element R with a small ionic radius R_i (e.g., $R = $ Yb, Lu) the effect of Pr on T_c is relatively small; e.g., for $x = 0.3$, T_c is suppressed only by 20%.[10] On the other hand, for the same Pr concentration $x = 0.3$ and for large Nd ($R = $ Nd) superconductivity is suppressed completely,[10] and bulk Néel order of the Cu and Pr spins sets in below T_N^{Cu} and T_N^{Pr}, respectively. Thus, in contrast to substitution of Cu by a $3d/4d$ element which directly and strongly perturbs the CuO_2 planes of the hole-doped cuprates,[16] the out-of-plane perturbation of the superconducting state by Pr is weaker and can be fine-tuned in a broad range by a hydrostatic or chemical pressure (i.e., by tuning R_i). Understanding of the suppression mechanisms of superconductivity in the $R_{1-x}Pr_xBa_2Cu_3O_{7-\delta}$ system, on the other hand, may help to clarify the pairing mechanisms in the cuprates.[17,18]

Soon after the discovery of the unusual behavior of Pr in the $R_{1-x}Pr_xBa_2Cu_3O_{7-\delta}$ system, the first theoretical explanations of this effect appeared. Fehrenbacher and Rice[19] proposed a strong hybridization of Pr with the neighboring O ions in the PE CuO_2 plane due to the large ionic radius of Pr. This

idea was further developed by Liechtenstein and Mazin.[20,21] However, there are difficulties in explaining the chemical and hydrostatic pressure effects in $R_{1-x}Pr_xBa_2Cu_3O_{7-\delta}$ by the hybridization model. Namely, a reduction of R_i should increase the hybridization and consequently reduce T_c which is in contrast to experimental observations.[10] Moreover, it was found that $PrBa_2Cu_3O_x$ single crystals prepared by the traveling-solvent floating-zone technique (TSFZ) or powders prepared by quick quenching from high temperatures may exhibit a substantial superconducting volume fraction with T_cs ranging from zero up to $\sim$85 K.[22–24] This finding was later interpreted as a novel realization of superconductivity mediated by strongly hybridized Pr-O bonds.[25]

Hydrostatic[26–29] and chemical[8,9,11,30] pressure effects (PEs) on T_c and the praseodymium Néel temperature T_N^{Pr} in $R_{1-x}Pr_xBa_2Cu_3O_{7-\delta}$ are quite controversial.[7,8] With increasing ionic radius R_i the transition temperature T_c of $R_{1-x}Pr_xBa_2Cu_3O_{7-\delta}$ gradually reduces and drops to zero (for $x \simeq 0.5$). Further increase of R_i leads to the onset of Néel order of Pr [see Fig. 7(a)]. A similar suppression of T_c is observed by the application of hydrostatic pressure P, suggesting an increased localization of carriers with P.[26–29] This effect becomes even stronger when x approaches x_{cr}.[31] Thus, for $x \simeq x_{cr}$ one expects an onset of Pr magnetic order and a complete suppression of superconductivity with increasing P [see Fig. 7(b)]. Surprisingly, though, a rather strong suppression of T_N^{Pr} was reported for $PrBa_2Cu_3O_{7-\delta}$[32] and $PrBa_2Cu_4O_8$[33] with $\partial T_N^{Pr}/\partial P \simeq -10$ K/GPa. These results indicate a delocalization of the carriers with P and suggest a complete suppression of T_N^{Pr} at $P \simeq 1.7$ GPa ($T_N^{Pr} \simeq 17$ K for $x = 1$). Furthermore, the superconducting crystals of $PrBa_2Cu_3O_x$ prepared by the TSFZ technique exhibit a positive hydrostatic pressure effect on T_c.[23,24] This observation can be interpreted as an extension of the phase diagram of T_N^{Pr} and T_c vs P, provided the samples prepared by the TSFZ technique experience an extra inhomogeneous chemical pressure caused by its microstructure which nearly suppresses T_N^{Pr} and partly recovers the superconducting state with a positive pressure effect on T_c (see Sec. IV for details).[8] In contrast to these reports, a small and positive PE on T_N^{Pr} was

detected by inelastic neutron scattering (INS) in single crystal $PrBa_2Cu_3O_x$.[34]

In order to clarify these controversial experimental results on the pressure effect we performed a muon spin rotation (μSR) study of the PE on T_N^{Pr} and T_N^{Cu} in $Nd_{1-x}Pr_xBa_2Cu_3O_{7-\delta}$ ($x = 0.3, 0.5, 0.7$, and 1) in the pressure range $0 < P < 2.4$ GPa. μSR is a sensitive microscopic probe for studying both magnetic and superconducting phases of a sample.[35,36] To minimize additional effects of chemical pressure, $R = $ Nd was chosen, since Nd and Pr are neighbors in the periodic table of elements and have nearly identical ionic radii.

We found an increase of T_N^{Pr} with increasing pressure at a rate $\simeq +0.7$ K/GPa for $0.3 < x < 1$ which is in contrast to previous reports,[32,33] but consistent with the negative hydrostatic PE on T_c and coincides with the result of PE on T_N^{Pr} determined with INS experiments,[34] suggesting an increased localization of the carriers with pressure. We do not observe any superconducting phase for pressures up to 2.3 GPa. In addition, the copper Néel temperature T_N^{Cu} was found also to increase with P.

The paper is organized as follows: Experimental details and sample preparation are described in Sec. II. In Sec. III we present results and details of the μSR data analysis. A discussion of the effect of hydrostatic pressure on the Cu and Pr Néel ordering in the magnetic part of the phase diagram is presented in Sec. IV, followed by the conclusions in Sec. V. Some zero- and transverse-field μSR results for the Co-Ni alloy (MP35N) used for the nonmagnetic pressure cells are presented in Appendix A. In Appendix B details of magnetization measurements are given.

II. EXPERIMENTAL DETAILS

High-quality polycrystalline $Nd_{1-x}Pr_xBa_2Cu_3O_{7-\delta}$ samples with $x = 0.3, 0.5, 0.7$, and 1 were prepared from Nd_2O_3, Pr_6O_{11}, CuO, and $BaCO_3$ of minimum purity of 99.99%, using a standard solid-state reaction. Proper amounts of the starting reagents were mixed and calcinated at temperatures 800–920 °C during at least 150 hours in air with several intermediate grindings. Finally, the as-prepared samples were oxidized in oxygen atmosphere at a pressure of 1 bar at 500 °C. Subsequently, the oxygen contents of the samples were determined to be close to 7 corresponding to $\delta \simeq 0.02$–0.05. Powder x-ray diffraction measurements which were carried on a D8 Advance Bruker AXS diffractometer using Cu K_α radiation indicate that the samples are single phase. The structural refinements were done using the program FULLPROF.[37] The results of these measurements and the refinement profiles are shown in Fig. 1. The lattice parameters of the $Nd_{1-x}Pr_xBa_2Cu_3O_{7-\delta}$ samples are in reasonable agreement with previous reports[11,38] and are summarized in Table I.

Zero-field (ZF) μSR experiments were performed at the μE1 beam line of the Paul Scherrer Institute (Villigen, Switzerland) using high-energy muons ($p_\mu \simeq 100$ MeV/c). The samples were cooled to $\simeq 3$ K, and μSR spectra were collected in a sequence with increasing temperature. Forward and backward positron detectors (relative to the polarization of the incident muon beam) were employed for the detection of the μSR asymmetry time spectrum $A(t)$.[35,36] Typical statistics for a μSR spectrum were 5×10^6 positron
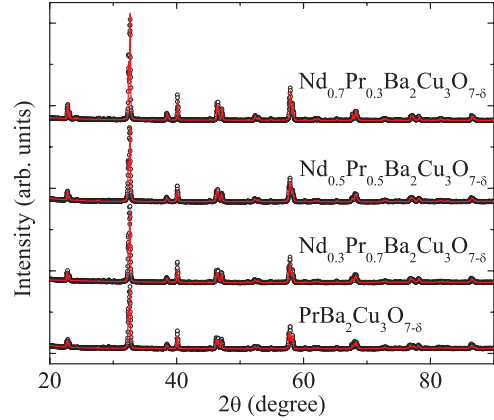

FIG. 1. (Color online) X-ray powder diffraction patterns for $Nd_{1-x}Pr_xBa_2Cu_3O_{7-\delta}$ ($x = 0.3, 0.5, 0.7$, and 1). The solid lines are fits to the data. The lattice constants are summarized in Table I.

events in the forward and the backward histograms. For the μSR studies pressure was applied with a piston-cylinder type pressure cell (μSR-PC) of alloy MP35N using Daphne pressure transmitting oil.[39] The maximum pressure attained was 2.4 GPa at 3 K. With increasing temperature the pressure increases gradually by $\simeq 0.3$ GPa at $T = 300$ K.[39] Thus, for the applied pressure 2.4 GPa at 3 K we have 2.7 GPa at 300 K. The actual pressure in the pressure cell was recorded by monitoring the superconducting transition of a small indium plate mounted in the μSR PC next to the sample (PE on T_c of In: $\partial T_c / \partial P = -0.364$ K/GPa).[40] In the following we refer to these measured pressures. Cold pressed samples of cylindrical shape with a size of 5×15 mm (diameter$\times$height) were used in order to achieve the highest filling factor of the μSR pressure cell. The fraction of the muons stopping in the sample was in the range 47–55%. The PE studies on the magnetization were performed in a commercial Quantum Design (MPMS) XL SQUID magnetometer using a diamond anvil type of pressure cell (DAPC) with a sample volume of $\simeq 0.1$ mm^3 (see Appendix B).

III. ANALYSIS AND RESULTS

The μSR data are well described in the entire temperature range with the following equation:[36]

$$A(t) = A_{pc}P_{pc}(t) + A_mP_m(t) + A_{pm}\exp(-\lambda_{pm}t). \quad (1)$$

The functions $P_\alpha(t)$ ($\alpha = $ pc, m) describe the muon polarization functions of the pressure cell (pc) and the magnetic fraction (m) of the sample, respectively (see below). The last term corresponds to the asymmetry function of the

TABLE I. Lattice constants of $Nd_{1-x}Pr_xBa_2Cu_3O_{7-\delta}$ for $x = 0.3$, 0.5, 0.7, and 1 obtained from powder x-ray diffraction measurements.

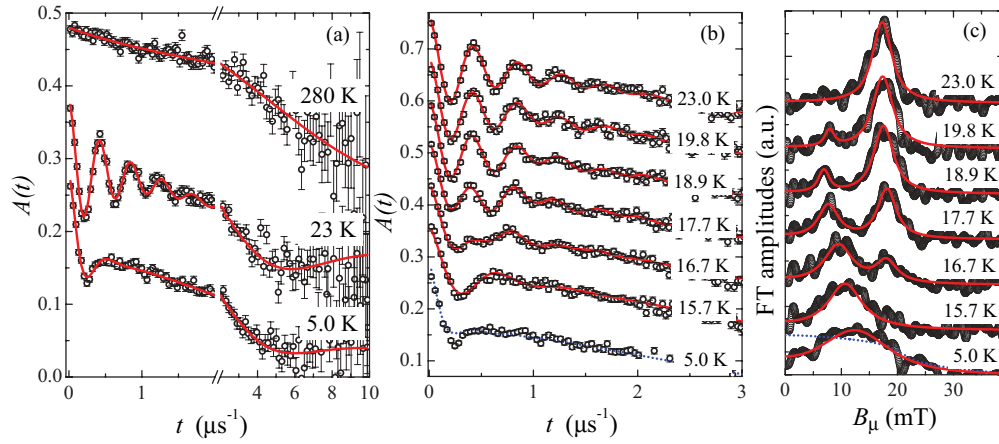| x	a (Å)	b (Å)	c (Å)
0.3	3.86078(8)	3.93271(16)	11.76732(42)
0.5	3.86191(12)	3.91003(14)	11.78065(44)
0.7	3.86288(10)	3.90871(11)	11.78923(32)
1	3.86429(8)	3.90624(9)	11.79748(23)

FIG. 2. (Color online) (a) Zero-field μSR time spectra $A(t)$ of PrBa$_2$Cu$_3$O$_{7-\delta}$ measured at $T = 5$, 23, and 280 K. The solid lines result from fitting Eqs. (1)–(3) to the data. For better visualization, the data measured at 23 and 280 K are shifted vertically by 0.1 and 0.2 units, respectively. (b) The same as in the panel (a) but for $T = 5$ K and in the temperature range of 15.7 to 23.0 K. For better visualization each spectrum is shifted vertically by 0.08 units. (c) Fourier transform (FT) of the spectra and the corresponding fitted curves shown in panels (a) and (b). The dotted lines in panels (b) and (c) are the best fit to the data and the FT of the Bessel function as described in the text.

paramagnetic (pm) fraction of the sample with a weak muon relaxation rate $\lambda_{\mathrm{pm}} \simeq 0.1$–$0.2$ μs^{-1}. The number of muons stopped in the pressure cell as well as the magnetic and the paramagnetic fractions of the sample are proportional to the initial asymmetries A_α (α = pc, m, and pm). The total initial asymmetry $A_{\mathrm{T}} = A_{\mathrm{pc}} + A_{\mathrm{m}} + A_{\mathrm{pm}} = 0.28$ and A_{pc} are temperature-independent constants. Typically, the fraction of muons stopped in the sample was $F_\mu = (A_{\mathrm{m}} + A_{\mathrm{pm}})/A_{\mathrm{T}} = 0.53$. The value of F_μ depends on the sample position and geometry with respect to muon beam[40,41] and is best determined in the temperature region 25–50 K, where the samples ($x = 1$, 0.7, and 0.5) exhibit a well-developed oscillating μSR time spectrum with a slow muon relaxation rate (see Fig. 2).

The muon polarization function of the pressure cell is described as follows (see also Appendix A):[40]

$$P_{\mathrm{pc}}(t) = \left[\frac{1}{3} + \frac{2}{3}\left(1 - \sigma_{\mathrm{pc}}^2 t^2\right)\exp\left(-\frac{1}{2}\sigma_{\mathrm{pc}}^2 t^2\right)\right]\exp(-\lambda_{\mathrm{pc}}t). \quad (2)$$

The relaxation rates of the pressure cell σ_{pc} and λ_{pc} are given in Appendix A.

The effect of pressure on the sample is reflected in the second and the third terms of Eq. (1). The second term has the form of the standard μSR depolarization function for a polycrystalline sample with internal field(s):[36,42,43]

$$P_{\mathrm{m}}(t) = \sum_{i=1}^{N} F_i^{\mathrm{m}}\left(\frac{1}{3} + \frac{2}{3}\cos(\gamma_\mu B_i t)e^{-\lambda_{\mathrm{T},i}t}\right)e^{-\lambda_{\mathrm{L}}t}. \quad (3)$$

Here, F_i^m represents the fraction of the signal related to the internal field B_i, $N = 1$ or 2 (see below), and $\gamma_\mu = 2\pi \times 135.53$ MHz/T is the gyromagnetic ratio of the muon. The parameters $\lambda_{\mathrm{T},i}$ and λ_{L} are the transverse and longitudinal muon relaxation rates of the i-th component. The longitudinal relaxation rate λ_{L} is related to spin dynamics and is absent in a statically ordered spin system while $\lambda_{\mathrm{T},i}$ is proportional to the field inhomogeneity at the muon site.[36] The weighting factors 1/3 and 2/3 in Eq. (3) originate from isotropic powder averaging of the μSR time spectra. Below we find that $\lambda_{\mathrm{T},i} \gg \lambda_{\mathrm{L}}$.

Results from fitting the μSR time spectra of PrBa$_2$Cu$_3$O$_{7-\delta}$ using Eqs. (1)–(3) at $T = 5$, 23, and 280 K are shown in Fig. 2(a). At 5 K a μSR time spectrum with fast relaxation was observed, consistent with a magnetic state of the sample. At 23 K an oscillating signal with slower relaxation is evident, similar to that observed in previous μSR studies.[42,43] At 280 K a slowly relaxing nonoscillating signal reflects the paramagnetic state of the sample. Figure 2(b) shows in more detail the evolution of the μSR spectra in the temperature range of 15.7 to 23 K where Pr-spin ordering occurs, and Fig. 2(c) presents the corresponding Fourier transform amplitudes which are described below.

The depolarization function $P_{\mathrm{m}}(t)$ given in Eq. (3) consists of two separate parts: a fraction $\frac{1}{3}$ that is slowly relaxing and nonoscillating, and a fraction $\frac{2}{3}$ that is oscillating. Hence, fitting Eqs. (1)–(3) to the data yields the nonoscillating fraction from the pressure cell, the 1/3 nonoscillating fraction from the sample, and the paramagnetic signal, all of which may be subtracted from the measured μSR signal. The Fourier transform (FT) of the remaining data represents the internal field distribution at the muon site(s) of the magnetic part of the sample, provided that the dynamic relaxation rate is negligible, $\lambda_L \ll \lambda_T$.[36,44] The result of this Fourier transformation for $x = 1$ and $P = 0$ in the temperature range 15.7 to 23 K is shown in Fig. 2(c). It is noteworthy that the results are only weakly dependent on the quality of the fit, since even a FT of the raw experimental data without subtraction of the nonoscillating components yields a very similar result, except for an additional contribution of the FT amplitudes around zero field. Figure 3 shows the FT amplitude color maps as a function of field and temperature of the whole experimental data at different x and P providing a quick and analysis-independent overview of the experimental results for the internal fields probed by μSR. For the sample with $x = 1$ a sudden decrease of the internal fields around 16–20 K [see Figs. 3(a)–3(c)] can clearly be seen, also observed in the previous μSR studies.[42,43] This drop reflects the Néel transition temperature of the Pr sublattice $T_{\mathrm{N}}^{\mathrm{Pr}}$.
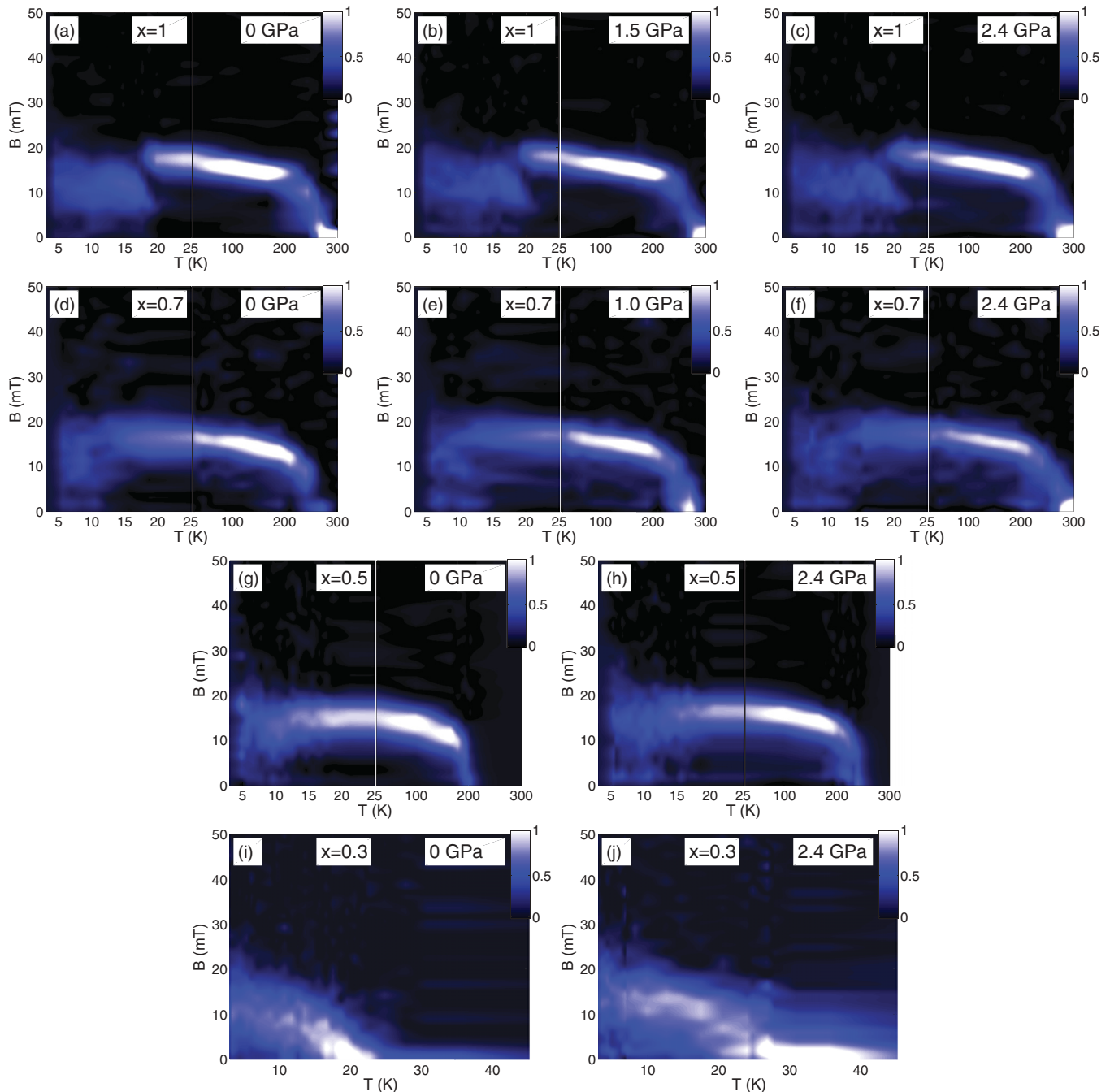
FIG. 3. (Color online) Fourier transform amplitudes of the oscillating components of the μSR time spectra as a function of field and temperature (color maps). Panels (a)–(c) correspond to $PrBa_2Cu_3O_{7-\delta}$ at $P = 0$, 1.52, and 2.4 GPa, respectively. Panels (d)–(f) correspond to $Pr_{0.7}Nd_{0.3}Ba_2Cu_3O_{7-\delta}$ at $P = 0$, 1.0, and 2.4 GPa, respectively; panels (g) and (h) to $Pr_{0.5}Nd_{0.5}Ba_2Cu_3O_{7-\delta}$ at $P = 0$ and 2.4 GPa; panels (i) and (j) to $Pr_{0.3}Nd_{0.7}Ba_2Cu_3O_{7-\delta}$ at $P = 0$ and 2.4 GPa. The amplitudes of the Fourier components were obtained from the raw data as described in the text.

A more detailed investigation of the data from the sample with $x = 1$, however, reveals two oscillating signals with distinct internal fields in the temperature range 16–20 K, pointing to a first-order magnetic transition [see Fig. 2(c)]. Below $T \simeq 16$ K a single fast relaxation is manifest in the μSR signal, which in the analysis emerges as a broad distribution of internal fields [see Figs. 2(a)–2(c) and 3(a)–3(c)]. At higher temperatures ($T > 25$ K) again a single internal field with a narrow distribution is evident, i.e., a slow transverse relaxation

rate, which gradually drops to zero around the Néel ordering temperature of the copper sublattice $T_N^{Cu} \simeq 270$ K. The field at the local muon site ($B \simeq 18.5$ mT at 23 K) is of the same magnitude as previously reported,[42,43] corresponding to a single muon stopping site as suggested for $PrBa_2Cu_3O_{7-\delta}$.[45]

Early neutron diffraction experiments revealed a simple commensurate antiferromagnetic order below 17 K in $PrBa_2Cu_3O_{7-\delta}$ with a magnetic moment direction along the c axis.[46] Later experiments showed a strong coupling between

the Pr- and Cu-spin sublattices with Pr ordering accompanied by a counterrotation of the Cu antiferromagnetism.[47] X-ray magnetic scattering points to incommensurate order of the Cu- and the Pr-spins with a long period of modulation.[48,49] In Fig. 2 we observe a muon depolarization with a small transverse relaxation rate at $T = 23$ K, consistent with commensurate antiferromagnetism.[50] However, well below T_N^{Pr} the relaxation rate increases strongly, and a broad distribution of internal fields is evident (see Fig. 2). This broad distribution indicates a quite disordered magnetic state of the sample.
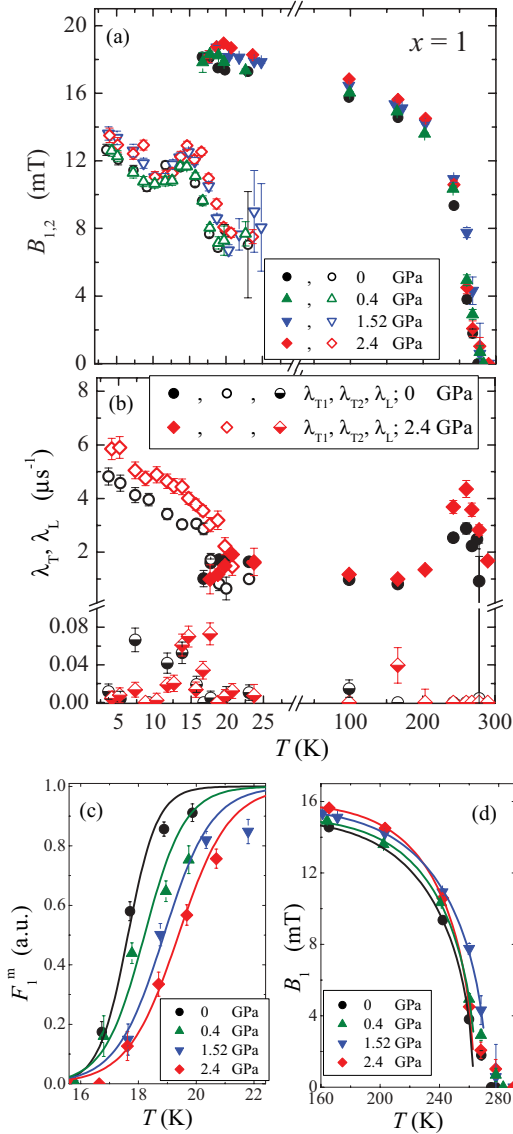

FIG. 4. (Color online) (a) The mean internal fields B_1 (full symbols) and B_2 (empty symbols) in PrBa$_2$Cu$_3$O$_{7-\delta}$ obtained with Eqs. (1)–(3) at $P = 0$, 0.4, 1.52, and 2.4 GPa. (b) Transverse (λ_{T1}, λ_{T2}) and longitudinal (λ_L) relaxation rates as a function of temperature for $P = 0$ and 2.4 GPa (the data for $P = 0.4$ and 1.52 GPa are not shown, since they are similar). (c) Temperature dependence of the magnetic fraction F_1^m, corresponding to the volume fraction of the sample with local field B_1 (see text). The solid lines represent best fits to the data using Eq. (5). (d) Temperature dependence of B_1 in the vicinity of T_N^{Cu}. The solid lines are best fits to the data using Eq. (4).

Strongly coupled Cu- and Pr-spin sublattices with identical incommensurate modulation periods should give rise to an incommensurate modulation of the magnetic field at the muon site, leading to a muon depolarization described by the spherical Bessel function of the first kind $j_0(x)$ [cos($\gamma_\mu B_i t$) in Eq. (3) is replaced with $j_0(\gamma_\mu B_i t)$, where $j_0(x) = \sin x/x$].[36] However, Eqs. (1)–(3) describe the data significantly better than the Bessel function [see Fig. 2(b)]. A Bessel function implies a broad distribution of internal fields with a cutoff[36] [see Fig. 2(c)]. But we observe a symmetric Gaussian-like distribution of fields.

For the samples with $x = 0.3$, 0.5, and 0.7 a single component of Eq. (3) suffices to describe the μSR time spectra in the whole temperature range [i.e., $N = 1$ in Eq. (3)]. At the corresponding T_N^{Pr} and below, the mean internal field does not exhibit a sudden drop [see Figs. 3(d)–3(j)], but decreases gradually with a substantial concurrent broadening of the internal field distribution. At temperatures above T_N^{Pr} the mean internal field decreases with increasing temperature and vanishes above the corresponding T_N^{Cu}. In the following sections we describe in more detail the results of the analysis for each of the samples.

A. Results for PrBa$_2$Cu$_3$O$_{7-\delta}$

The analysis of the μSR spectra of PrBa$_2$Cu$_3$O$_{7-\delta}$ showed that at zero pressure two distinct local fields could be identified in the temperature range $16 < T < 23$ K, where the onset of magnetic ordering of the Pr sublattice $T_N^{Pr} \simeq 17$ K occurs (see Fig. 3). Below 16 K and above 23 K only a single local field is present. Indices $i = 1,2$ in Eq. (3) refer to properties of the μSR signals in the high and the low temperature ranges, respectively. Notations in Eq. (3) are as follows: local fields B_1 and B_2; transverse relaxation rates λ_{T1} and λ_{T2}; weight functions F_1^m and F_2^m.

The temperature dependence of the mean local field in PrBa$_2$Cu$_3$O$_{7-\delta}$ was obtained by fitting Eqs. (1)–(3) to the data for pressures $P = 0$, 0.4, 1.52, and 2.4 GPa, as shown in Figs. 4(a) and 4(d). The local field B_2 has a nonzero value at temperatures above T_N^{Pr} [see Figs. 3(a)–3(c)] and increases with decreasing temperature. At temperatures around T_N^{Pr} this increase is not monotonic, but exhibits a pronounced peak for all applied pressures $P = 0$, 0.4, 1.52, and 2.4 GPa.

In the high-temperature range field B_1 attains its maximum at around 20 K ($B_1 \simeq 18$ mT). With increasing temperature the magnitude of B_1 gradually decreases and finally vanishes at about 270 K, corresponding to the Néel transition temperature of the Cu spin sublattice T_N^{Cu}.[42,43] In order to determine T_N^{Cu} a power-law function was fitted to the data for B_1 above 150 K:

$$B(T) = B_0 \left(1 - \left(\frac{T}{T_N^{Cu}}\right)^p\right)^q, \qquad (4)$$

where the value of q was fixed to 0.5 for all the samples and pressures. In Table II the values of T_N^{Cu} are summarized for all pressures applied.

The transverse muon relaxation rates λ_{T1} and λ_{T2}, characterizing the distribution of local fields,[36] are shown in Fig. 4(b). For $T < 220$ K the relaxation rate λ_{T1} is small ($\lambda_{T1} \simeq 1.21$ μs^{-1}) and at $T \simeq T_N^{Cu}$ a peak in λ_{T1} is observed. The relaxation rate λ_{T2} increases monotonically with decreasing

temperature below T_N^{Pr}, which is also evident in the Fourier amplitudes of the raw experimental data [see Figs. 3(a)–3(c)]. The amplitudes of the Fourier components gradually decrease below T_N^{Pr}, whereas the width of the field distribution increases. The longitudinal relaxation rate λ_L, characterizing the muon spin relaxation due to fluctuating magnetic fields, is quite small in the whole temperature range [see Fig. 4(b)].

As pointed out above the variation of the local fields B_1 and B_2 at T_N^{Pr} is discontinuous at all pressures for 16 K < T < 23 K, suggesting an inhomogeneous transition from the Cu to the Cu + Pr sublattice magnetic order with decreasing temperature [see Fig. 2(c)]. For a spatially homogeneous transition a gradual broadening of the local field is expected due to fluctuations of the magnetic order parameter. The discontinuity is presumably caused either by an electronic inhomogeneity or by an inhomogeneity of the local chemical pressure. The

corresponding weight functions of the two signals are F_i^m ($i = 1,2$) (with $F_1^m + F_2^m = 1$), each of which represents a volume fraction of the sample with the local field B_i. Figure 4(c) shows the temperature dependence of F_1^m for $P = 0$, 0.4, 1.52, and 2.4 GPa. Fitting the phenomenological equation

$$F(T) = A \left(1 - \frac{1}{\exp\left(\frac{T - T_N}{\Delta T}\right) + 1} \right) + D \quad (5)$$

to the data with $D = 0$ and $A = 1$, one obtains the solid lines in Fig. 4(c). Here, the parameter A describes the maximal value of F_1^m while the ΔT is proportional to width of the magnetic transition. Note that the second term in the parentheses resembles the Fermi function. The Néel transition temperature of praseodymium ($T_N^{Pr} = T_N$) was determined from the measured values of F_1^m by means of Eq. (5) in the vicinity of the
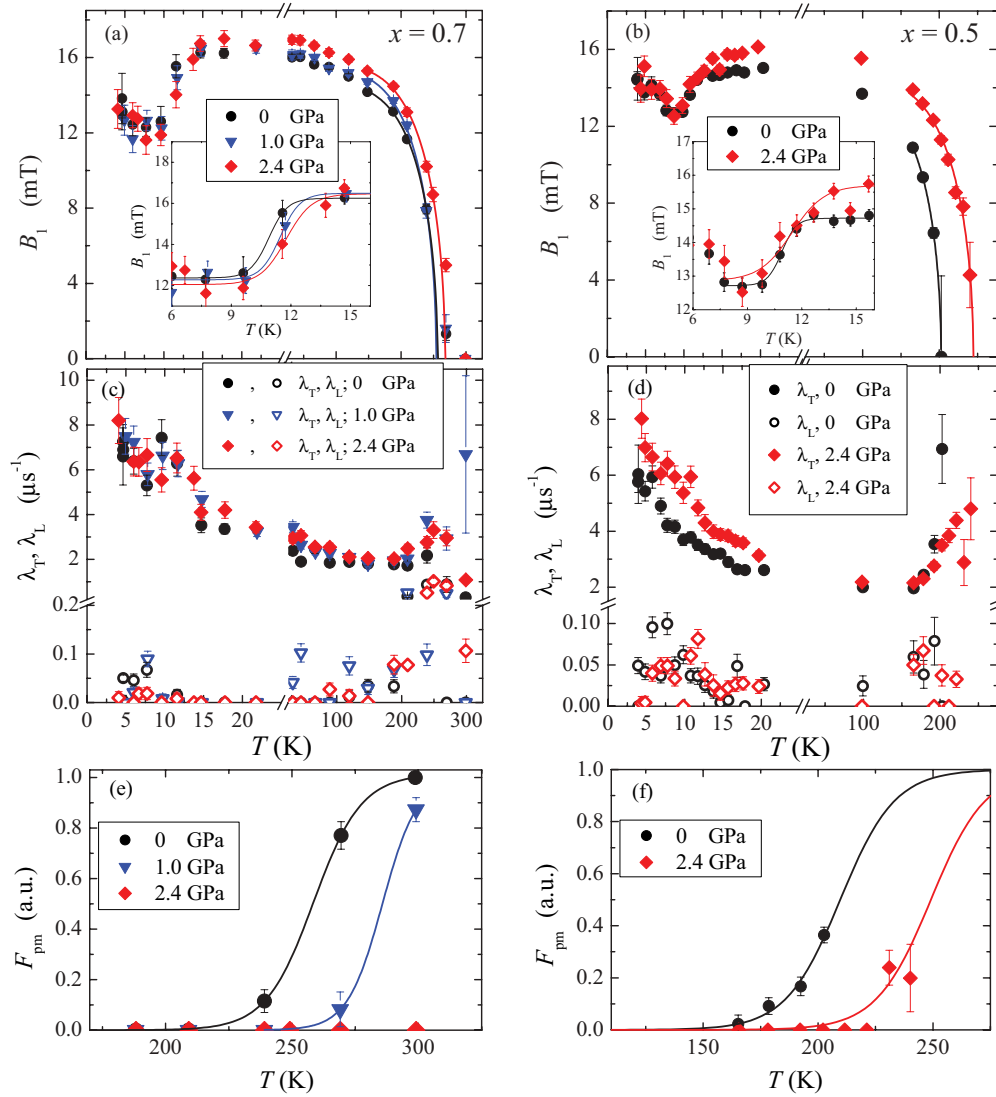

FIG. 5. (Color online) (a) The mean internal field B_1 in $Nd_{0.3}Pr_{0.7}Ba_2Cu_3O_{7-\delta}$ obtained with Eqs. (1)–(3) at applied pressures $P = 0$, 1.0, and 2.4 GPa. (b) The same as panel (a), but for sample $Nd_{0.5}Pr_{0.5}Ba_2Cu_3O_{7-\delta}$ at $P = 0$ and 2.4 GPa. The solid lines in (a) and (b) correspond to the best fits to the data using Eq. (4). The inserts in (a) and (b) show B_1 in the vicinity of T_N^{Pr} with solid lines representing best fits to the data using Eq. (5). (c) and (d) The corresponding transverse (λ_T) and longitudinal (λ_L) relaxation rates as a function of temperature for $Nd_{0.3}Pr_{0.7}Ba_2Cu_3O_{7-\delta}$ and $Nd_{0.5}Pr_{0.5}Ba_2Cu_3O_{7-\delta}$, respectively. (e) and (f) Temperature dependence of the paramagnetic fraction F_{pm} in $Nd_{0.3}Pr_{0.7}Ba_2Cu_3O_{7-\delta}$ and $Nd_{0.5}Pr_{0.5}Ba_2Cu_3O_{7-\delta}$, respectively. The solid lines are results from fitting Eq. (5) to the data.

TABLE II. Néel temperatures for copper (T_N^{Cu}) and praseodymium (T_N^{Pr}) in $Nd_{1-x}Pr_xBa_2Cu_3O_{7-\delta}$ ($x = 0.3$, 0.5, 0.7, and 1.0) at various pressures. In addition, the values of T_N^{Cu*} extracted from the data of the samples with $x = 0.3$, 0.5, and 0.7 are listed (see text for an explanation).

x	P (GPa)	T_N^{Pr} (K)	T_N^{Cu} (K)	T_N^{Cu*} (K)
1	0	17.6(1)	262.8(10)	
1	0.4	18.2(2)	264.7(10)	
1	1.52	18.9(1)	271.6(10)	
1	2.4	19.4(1)	263.1(10)	
0.7	0	10.9(2)	256(2)	258(3)
0.7	1.0	11.5(2)	254(2)	285(3)
0.7	2.4	11.8(2)	267(3)	>300
0.5	0	10.9(1)	202(3)	209.6(10)
0.5	2.4	11.4(5)	244.4(10)	249(5)
0.3	0	3(1)	19.9(2)	21.1(5)
0.3	2.4	5(1)	27.1(2)	36.2(5)

transition. Since we have a gradual onset of Pr magnetic order this definition of T_N^{Pr} corresponds to the temperature where half of the sample volume fraction is in the Pr-ordered state. The width of this transition is described by the parameter $\Delta T = 0.5, 0.7, 0.8$, and 0.9 K at $P = 0, 0.4, 1.52$, and 2.4 GPa, respectively. The results for T_N^{Pr} are summarized in Table II.

B. Results for $Nd_{0.3}Pr_{0.7}Ba_2Cu_3O_{7-\delta}$ and $Nd_{0.5}Pr_{0.5}Ba_2Cu_3O_{7-\delta}$

The temperature dependence of the mean local field B_1 in $Nd_{0.3}Pr_{0.7}Ba_2Cu_3O_{7-\delta}$ for $P = 0, 1.0$, and 2.4 GPa and in $Nd_{0.5}Pr_{0.5}Ba_2Cu_3O_{7-\delta}$ for $P = 0$ and 2.4 GPa, obtained by fitting Eqs. (1)–(3) to the data, is shown in Figs. 5(a) and 5(b), respectively.

In contrast to $PrBa_2Cu_3O_{7-\delta}$, the μSR spectra for the two Nd-substituted samples are well described with a single internal field in the whole temperature range at all pressures applied, but two distinct temperature regions are evident. For $T > 15$ K the local internal field gradually decreases with increasing temperature from $B \simeq 16$ mT and vanishes around $T \simeq 260$ K ($T \simeq 200$–250 K) in $Nd_{0.3}Pr_{0.7}Ba_2Cu_3O_{7-\delta}$ ($Nd_{0.5}Pr_{0.5}Ba_2Cu_3O_{7-\delta}$). This temperature corresponds to T_N^{Cu} and was determined by fitting Eq. (4) to the data above 150 K with $q = 0.5$. The corresponding curves are shown as solid lines in Figs. 5(a) and 5(b). The values of T_N^{Cu} for $Nd_{0.3}Pr_{0.7}Ba_2Cu_3O_{7-\delta}$ ($Nd_{0.5}Pr_{0.5}Ba_2Cu_3O_{7-\delta}$) for $P = 0$, 1.0, and 2.4 GPa ($P = 0$ and 2.4 GPa) are given in Table II.

In the low-temperature region ($T < 15$ K) the mean local field B_1 drops for both samples from $B \simeq 16.5$ mT to $B \simeq 12$ mT at $T_N^{Pr} \simeq 11$ K. As is evident from Figs. 3(d)–3(h), 5(a), and 5(b), the transition is smoother with a substantial broadening of the field distribution below T_N^{Pr}. In order to determine T_N^{Pr}, the data points in the vicinity of the T_N^{Pr} were analyzed with Eq. (5). The results of this analysis are represented by the solid lines in the insert of Fig. 5(a) for $Nd_{0.3}Pr_{0.7}Ba_2Cu_3O_{7-\delta}$ and Fig. 5(b) for $Nd_{0.5}Pr_{0.5}Ba_2Cu_3O_{7-\delta}$. The corresponding Néel temperatures T_N^{Pr} are listed in Table II.

The transverse (λ_T) and longitudinal (λ_L) relaxation rates for $Nd_{0.3}Pr_{0.7}Ba_2Cu_3O_{7-\delta}$ and $Nd_{0.5}Pr_{0.5}Ba_2Cu_3O_{7-\delta}$ are shown in Fig. 5(c) and Fig. 5(d), respectively. The random
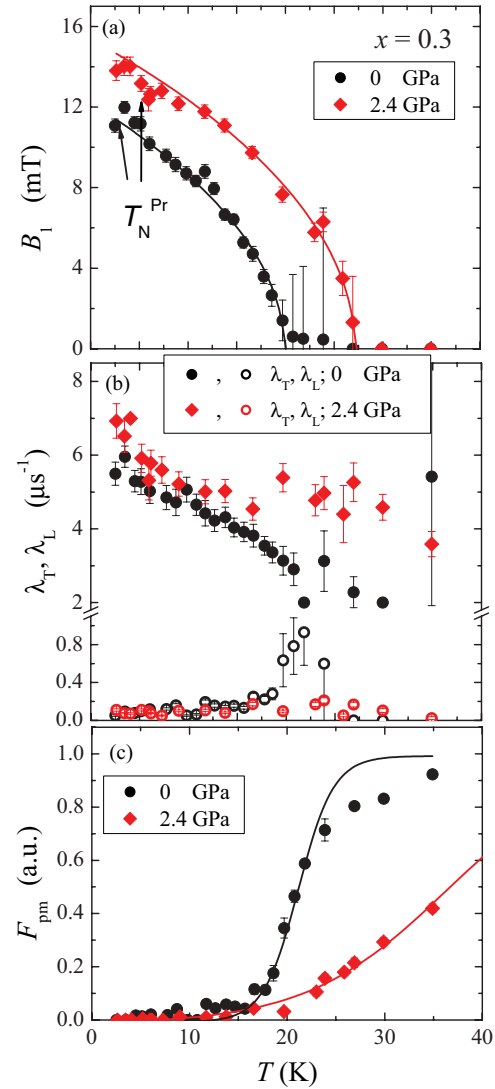

FIG. 6. (Color online) (a) The mean internal field B_1 in $Nd_{0.7}Pr_{0.3}Ba_2Cu_3O_{7-\delta}$ obtained with Eqs. (1)–(3) at $P = 0$ and 2.4 GPa. The solid lines represent best fits to the data using Eq. (4). The arrows indicate possible antiferromagnetic transitions at T_N^{Pr}. (b) Corresponding transverse (λ_T) and longitudinal (λ_L) relaxation rates as a function of temperature for $P = 0$ and 2.4 GPa. (c) Temperature dependence of the paramagnetic fraction F_{pm}. The solid lines are best fits to the data using Eq. (5).

occupation of Nd^{3+} ions at the praseodymium sites gives rise to an additional disorder of the local fields that is perceived by the muon. Thus, the transverse relaxation rate λ_T becomes substantially larger than for $PrBa_2Cu_3O_{7-\delta}$ ($x = 1$). The longitudinal relaxation rate λ_L is small in the whole temperature range studied, except for $T \simeq T_N^{Cu}$, where λ_L exhibits a peak.

In contrast to $PrBa_2Cu_3O_{7-\delta}$, the transition between the magnetically ordered and the paramagnetic state around T_N^{Cu} is gradual for the samples with $x < 1$. With increasing temperature the mean local field B_1 vanishes at T_N^{Cu}. Above T_N^{Cu}, however, a fraction of the μSR signal still exhibits a substantial transverse relaxation rate λ_T with zero mean field, suggesting the presence of quasistatic and disordered

magnetic fields at the muon site. Below T_N^{Cu} a fraction of the sample is in the paramagnetic state for which the relaxation rate is small: $\lambda_{pm} \simeq 0.1 - 0.2$ μs^{-1}. Thus, two distinct values of T_N^{Cu} may be identified: (1) the temperature where the mean local field B_1 vanishes, and (2) the temperature where a fraction of one half of the sample volume is in the paramagnetic state. Close to T_N^{Cu} the temperature-independent asymmetry of the sample, $A_s = A_m + A_{pm}$, may therefore be written as $A_m = A_s(1 - F_{pm})$ and $A_{pm} = A_s F_{pm}$, where the parameter F_{pm} is the volume fraction of the sample in the paramagnetic state ($0 \leqslant F_{pm} \leqslant 1$). Figures 5(e) and 5(f) show the temperature dependence of F_{pm} at different pressures for $Nd_{0.3}Pr_{0.7}Ba_2Cu_3O_{7-\delta}$ and $Nd_{0.5}Pr_{0.5}Ba_2Cu_3O_{7-\delta}$, respectively. The solid lines represent fits of Eq. (5) to the data with $A = 1$ and $D = 0$. The Néel temperature obtained from the temperature dependence of F_{pm} for various pressures and substitution fractions x is denoted as T_N^{Cu*}, and the corresponding values of T_N^{Cu*} are listed in Table II.

C. Results for $Nd_{0.7}Pr_{0.3}Ba_2Cu_3O_{7-\delta}$

The temperature dependence of the mean local field B_1 in $Nd_{0.7}Pr_{0.3}Ba_2Cu_3O_{7-\delta}$ obtained by fitting Eqs. (1)–(3) to the data for $P = 0$ and 2.4 GPa is shown in Fig. 6(a). A single component in Eq. (3) is sufficient to describe the μSR time spectra in the whole temperature range. The local field B_1 increases monotonically with decreasing temperature, but without any pronounced signature at the onset of Pr Néel ordering. The minor features visible around 3 and 5 K for $P = 0$ and 2.4 GPa [shown by the arrows in Fig. 6(a)] are possible signs of Pr ordering, since for the samples with higher concentration of praseodymium ($x = 0.5$ and 0.7), a decrease of B_1 at T_N^{Pr} is concurrent with an increase of B_1 at lower temperatures [see Figs. 5(a) and 5(b)]. The solid lines in Fig. 6(a) represent best fits to the data using Eq. (4) with

$q = 0.5$. The transition temperatures T_N^{Cu} obtained from this analysis for both pressures $P = 0$ and 2.4 GPa are summarized in Table II. The corresponding transverse (λ_T) and longitudinal (λ_L) relaxation rates are depicted in Fig. 6(b). λ_T exhibits a monotonic decrease with increasing temperature, while λ_L at $P = 0$ GPa has a peak around T_N^{Cu}. The paramagnetic volume fraction for both pressures is shown in Fig. 6(c). Similar to the previous case ($x = 0.5$ and 0.7) F_{pm} increases gradually with increasing temperature. The width of this transition, however, gets broad at $P = 2.4$ GPa. The solid lines in Fig. 6(c) result from fitting Eq. (5) to the data with $A = 1$ and $D = 0$. The corresponding Néel temperatures T_N^{Cu*} are listed in Table II.

IV. DISCUSSION

Figure 7(a) shows the normalized superconducting (T_c / T_c^{max}) and magnetic ($T_N^{Pr} / T_N^{Pr,max}$) transition temperatures in $R_{1-x}Pr_xBa_2Cu_3O_{7-\delta}$ as a function of ionic radius R_i for $x = 0.5$ obtained in Ref. 10. With increasing ionic radius R_i of the rare-earth element superconductivity is suppressed. At a sufficiently large R_i superconductivity vanishes and Pr-magnetic order develops, crossing a region of coexistence of both phases.[10] For hydrostatic pressure a negative PE on T_c was reported for $R_{1-x}Pr_xBa_2Cu_3O_{7-\delta}$ at $x \lesssim x_{cr}$ which may be explained by the increased localization of carriers with P [see Fig. 7(b)].[26–29] The closer x is to the respective x_{cr} the stronger is the PE. There are no reports on PE on T_N^{Pr} for $x < 1$ at present. However, the results of the chemical PE [see Fig. 7(a)] and the increased localization of carriers with P suggest a positive PE on T_N^{Pr} after complete suppression of superconductivity. For $x = 1$, no and a small positive PE on T_N^{Pr} were found by transport and INS experiments, respectively.[34,51] In contrast, a negative PE on T_N^{Pr} was reported for $PrBa_2Cu_3O_{7-\delta}$[32] and $PrBa_2Cu_4O_8$[33] with a large
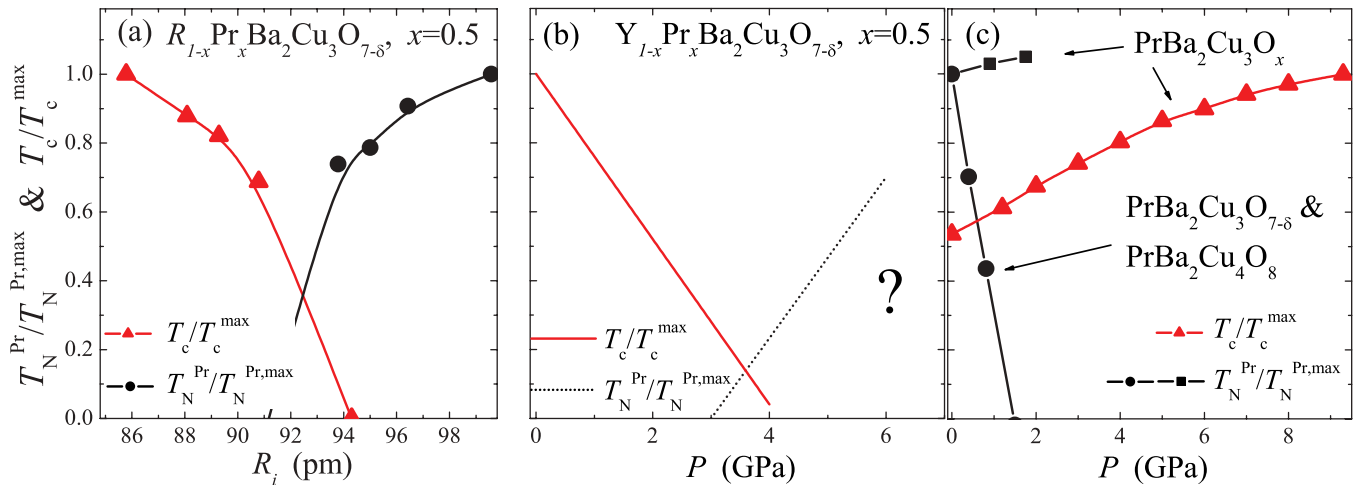
FIG. 7. (Color online) (a) T_c / T_c^{max} and $T_N^{Pr} / T_N^{Pr,max}$ of $R_{1-x}Pr_xBa_2Cu_3O_{7-\delta}$ as a function of the rare-earth ionic radius R_i for $x = 0.5$ with $T_c^{max} = 32.6$ K and $T_N^{max} = 12.1$ K (the data are from Ref. 10). (b) T_c / T_c^{max} for $x = 0.5$ and $R = $Y ($T_c^{max} = 28.9$ K; the data are from Ref. 26). For all rare-earth elements and $x \lesssim x_{cr}$ the pressure effect on T_c is negative (Refs. 26–29). The PE increases in magnitude with increasing x. No studies of the PE on T_N for $x < 1$ have been performed up to now (indicated by the question mark). The dotted line shows a possible scenario for the PE on T_N suggested by the results of chemical pressure effect [panel (a)]. (c) $T_N^{Pr} / T_N^{Pr,max}$ and T_c / T_c^{max} of $PrBa_2Cu_3O_x$ and $PrBa_2Cu_4O_8$ as a function of hydrostatic pressure. The results for T_N are from Refs. 32,33 (circles) with $T_N^{max} \simeq 17.5$ K and Ref. 34 (squares) with $T_N^{max} \simeq 19.6$ K. The pressure effect data on T_c for $PrBa_2Cu_3O_x$ are from Ref. 24 ($T_c^{max} \simeq 105$ K). The solid lines in panels (a), (b), and (c) are guides to the eye.

suppression rate: $\partial T_N^{Pr}/\partial P \simeq -10$ K/GPa [see Fig. 7(c)]. For $T_N^{Pr} = 17$ K a linear extrapolation suggests that for $P \gtrsim 1.7$ GPa the Pr Néel order might be suppressed completely, and followed by a transition to a superconducting phase. Indeed, in PrBa$_2$Cu$_3$O$_{7-\delta}$ thin-film,[22] polycrystalline,[52,53] and single-crystal[23,24] samples superconductivity with an unusually strong and positive effect of hydrostatic pressure[23,24] on T_c has been found. In Fig. 7(c) we show the results of Ref. 24. Figure 7(c) suggests that the observation of superconductivity in PrBa$_2$Cu$_3$O$_{7-\delta}$ samples might be related to a strong suppression rate of T_N^{Pr} with pressure, provided these superconducting samples have an extra initial chemical pressure/stress caused by a microstructure which partly suppresses magnetism.

The magnetic phase diagram for Pr (empty symbols) and Cu (full symbols) in the doping range $0.3 < x < 1$ is given in Fig. 8, showing the Néel transition temperatures T_N^{Pr} and T_N^{Cu} at pressures 0 and 2.4 GPa. For $x = 1$ the PE on T_N^{Cu} is rather small. The PE increases gradually with x, and attains a maximum for $x \simeq 0.5$. For $x = 0.3$ the effect of hydrostatic pressure on T_N^{Cu} is again small in absolute numbers, but large on a relative scale [see Fig. 9(a)]. Of the several factors determining T_N^{Cu} the following deserve attention: (1) the effective charge carrier concentration n_h in the CuO$_2$ planes, and (2) the in-plane and out-of-plane exchange integrals for the Cu spins. The former leads to a reduction of the T_N^{Cu} due to disorder introduced by the localized or hopping carriers in the antiferromagnetic background of the Cu spins. The latter determine the Néel transition temperature for a system without charge carriers. Both factors are pressure dependent. Praseodymium ions localize the carriers in the CuO$_2$ planes, resulting in a reduction of the effective carrier concentration n_h that in turn leads to a suppression of superconductivity (or increase of T_N^{Cu}). This "localization efficiency" strongly depends on chemical pressure,[10] and it is natural to assume that it is also strongly pressure dependent. On the other hand, with increasing pressure an additional charge transfer to the CuO$_2$ planes takes place in the YBa$_2$Cu$_3$O$_x$ system,[54–56] leading to an increase of the maximal superconducting transition
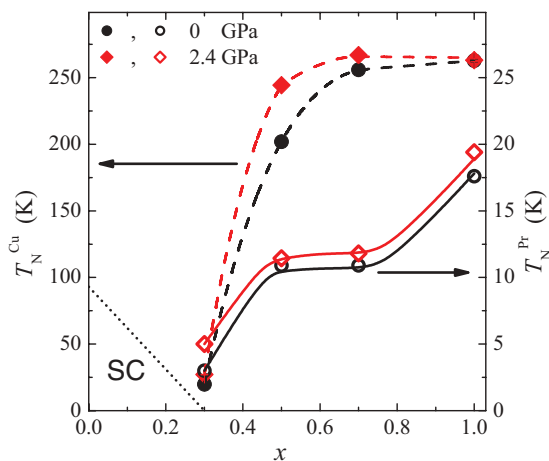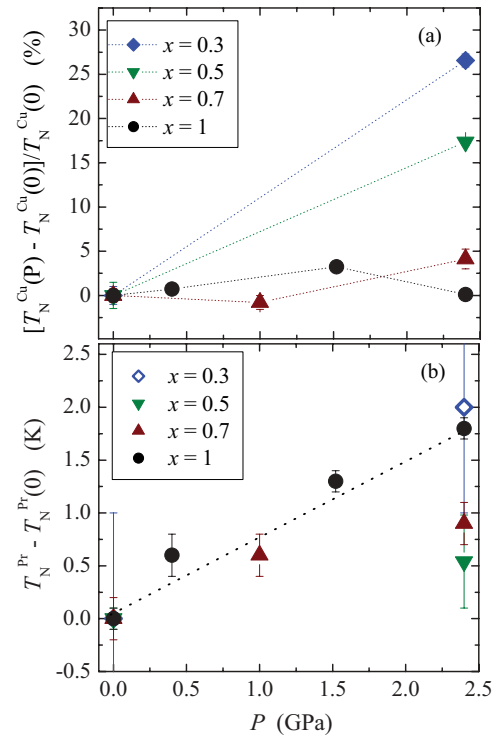

FIG. 9. (Color online) (a) Relative change of the copper Néel temperature T_N^{Cu} in Nd$_{1-x}$Pr$_x$Ba$_2$Cu$_3$O$_{7-\delta}$ as a function of pressure for $x = 0.3$, 0.5, 0.7, and 1. (b) Change of the praseodymium Néel temperature T_N^{Pr} in Nd$_{1-x}$Pr$_x$Ba$_2$Cu$_3$O$_{7-\delta}$ as a function of pressure for $x = 0.3$, 0.5, 0.7, and 1. The data for $x = 0.3$ are shown as empty symbols, since the uncertainty in T_N^{Pr} is rather large. The dotted lines are guides to the eye.

temperature with increasing pressure, or in a different perspective to a decrease of the magnetic transition temperature. For $x > 0.7$ the value of T_N^{Cu} only weakly depends on x, suggesting a saturation of the suppression of n_h by Pr (see Fig. 8). Therefore, the effective charge concentration is too small to influence T_N^{Cu} for $x > 0.7$ at zero pressure. T_N^{Cu} for $x = 1$ increases with increasing pressure up to 1.5 GPa, and then decreases again for still higher pressures. Consequently, the weak and nonlinear pressure dependence of T_N^{Cu} for $x = 1$ is predominantly determined by the PE on the exchange integrals of the Cu spins. The variation of T_N^{Cu} with pressure is substantially stronger for $x = 0.5$ than for $x = 1$. For $x = 0.5$ at zero pressure, T_N^{Cu} is reduced compared to $x = 1$ due to the presence of charge carriers. Thus, the positive PE on T_N^{Cu} is substantially influenced by the negative PE on the effective carrier concentration obviously dominating for $x = 0.5$.

The Néel temperature T_N^{Pr} at 0 and 2.4 GPa is shown as a function of Pr concentration x in Fig. 8. At zero pressure the values of T_N^{Pr} are in good agreement with previous reports.[10,42,43] In Fig. 9(b) the variations of T_N^{Pr} for all pressures investigated and all samples are shown. The PE on T_N^{Pr} is positive ($\simeq + 0.7$ K/GPa) for all the praseodymium concentrations ($0.3 < x < 1$).

The present results for the PE on both T_N^{Cu} and T_N^{Pr} suggest an increased localization of carriers with P and drastically differ from those reported previously for PrBa$_2$Cu$_3$O$_{7-\delta}$[32] and PrBa$_2$Cu$_4$O$_8$,[33] as obtained by magnetization measurements

FIG. 8. (Color online) Phase diagram of Cu (full symbols) and Pr (empty symbols) magnetic order in Nd$_{1-x}$Pr$_x$Ba$_2$Cu$_3$O$_{7-\delta}$ ($x = 0.3$, 0.5, 0.7, and 1) at pressures of 0 and 2.4 GPa. The dotted line indicates the superconducting transition (see Ref. 10). Solid and dashed lines are guides to the eye.

under pressure. It contrasts also with the positive hydrostatic PE on T_c found in superconducting PrBa$_2$Cu$_3$O$_{7-\delta}$ (see Fig. 7).[23,24] Our magnetization measurements of PrBa$_2$Cu$_3$O$_{7-\delta}$ under hydrostatic pressures up to 2.3 GPa could not reveal a Meissner fraction (with a precision better than 1%), confirming absence of superconductivity in the present samples (see Appendix B). The positive PE on T_N^{Pr} and T_N^{Cu} found for $x_{cr} \lesssim x < 1$ is, however, in good agreement with the results of INS experiments[34] and consistent with the negative effect of hydrostatic pressure reported for R_{1-x}Pr$_x$Ba$_2$Cu$_4$O$_8$ at $x \lesssim x_{cr}$.[26–29] The suppression of superconductivity and the onset of magnetism with P are in accord with the similar behavior of T_c and T_N^{Pr} in R_{1-x}Pr$_x$Ba$_2$Cu$_4$O$_8$ as a function of chemical pressure [see Fig. 7(a)].[10] Our findings are also in agreement with Ref. 51, where T_N^{Pr} was identified from transport measurements for Y$_{1-x}$Pr$_x$Ba$_2$Cu$_4$O$_8$, at pressures up to 1 GPa, and found to be pressure independent. Therefore, our results strongly suggest an increased localization of the carriers in Nd$_{1-x}$Pr$_x$Ba$_2$Cu$_3$O$_{7-\delta}$ by Pr^{3+} with the application of hydrostatic pressure up to 2.4 GPa, even for $x = 1$. Further reliable measurements of the PE on T_N^{Pr} are needed to verify the results of Refs. 32,33. We think that a positive PE on T_c, suggesting delocalization of carriers with pressure, found in single-crystal samples of PrBa$_2$Cu$_3$O$_{7-\delta}$ is exceptional and is related to details of their microstructure.

V. CONCLUSIONS

We investigated the effect of pressure on the Pr and Cu Néel magnetic order in Nd$_{1-x}$Pr$_x$Ba$_2$Cu$_3$O$_{7-\delta}$ for $x = 0.3, 0.5, 0.7$, and 1. In several aspects the present results differ drastically from those reported previously.[32,33] The effect of pressure on the Pr Néel ordering temperature T_N^{Pr} was found to be positive for all the investigated Pr concentrations x, amounting to $\simeq +0.7$ K/GPa. This finding is in agreement with the negative effect of pressure on the superconducting transition temperature T_c observed for $0.1 < x < 0.3$ and coincides with the result of inelastic neutron scattering experiments.[34] This implies a reduction of the effective charge concentration with pressure, resulting in a suppression of T_c and an increase of

T_N^{Pr} (for $x > 0.3$).[27] In PrBa$_2$Cu$_3$O$_{7-\delta}$ the effect of pressure on the Néel ordering temperature T_N^{Cu} for the Cu sublattice is weak and nonlinear, suggesting a small pressure dependence of the in- and out-of-plane exchange integrals for the Cu spins. Thus, the strong effect of pressure on T_N^{Cu} for $0.3 < x < 0.5$ is dominated by a reduction of the effective charge concentration in the CuO$_2$ planes with pressure.

APPENDIX A: μSR SPECTRA OF THE Co-Ni ALLOY (MP35N)

The nonmagnetic Co-Ni alloy (MP35N) used for high-pressure μSR studies is composed of 35% Co, 35% Ni, 20% Cr, and 10% Mo (by weight).[40] For temperatures above 2 K the parameters of the μSR spectra may vary within a range of $\sim$10%, depending on preparation and aging procedures. Below 2 K this variation can be more pronounced. In the temperature range of 2 to 100 K the μSR spectra are practically temperature independent (for details see Ref. 40). Here we present the results for zero and weak transverse field μSR of MP35N in the broad temperature range of 5 to 300 K. The zero-field μSR spectra are well described by Eq. (2).[40] For a transverse field B, the muon depolarization may be analyzed with the function

$$P_{\mathrm{pc,TF}}(t) = \cos(\gamma_\mu B t + \phi) \exp\left(-\tfrac{1}{2}\sigma_{\mathrm{pc}}^2 t^2\right) \exp(-\lambda_{\mathrm{pc}} t). \quad \text{(A1)}$$

Here, σ_{pc} and λ_{pc} are the Gaussian and exponential muon relaxation rates, while ϕ is the initial phase of the muon polarization. A weak transverse field of $B = 30$ mT was used for these tests.
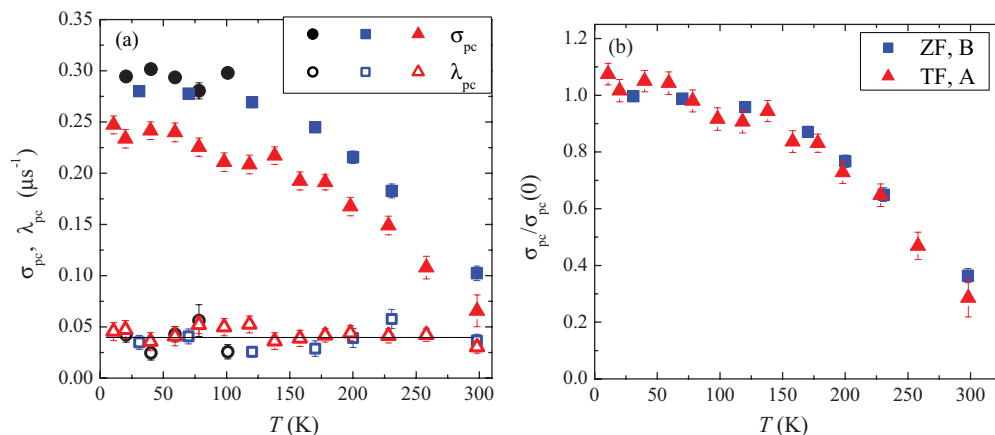

FIG. 10. (Color online) (a) Gaussian (σ_{pc}, full symbols) and exponential (λ_{pc}, empty symbols) relaxation rates of MP35N for sample A (circles, triangles) and B (squares) measured in transverse- (triangles) and zero-field (circles, squares) modes. The solid horizontal line represents the mean value of $\lambda_{\mathrm{pc}} = 0.04\ \mu$s^{-1}. (b) Normalized Gaussian muon relaxation rate $\sigma_{\mathrm{pc}}(T)/\sigma_{\mathrm{pc}}(0)$ for sample A in the transverse field mode and for sample B in the zero-field mode.

Two different samples of MP35N were tested, here referred to as A and B. Both samples were taken from the same batch, but were subjected to different thermal aging processes. The parameters σ_{pc} and λ_{pc} for both samples as obtained with Eqs. (2) and (A1) for zero and transverse fields in the temperature range of 5 to 300 K are presented in Fig. 10(a). The exponential shapes of the relaxation rate dependence λ_{pc} are identical for both samples in zero and transverse field with the temperature-independent value $\lambda_{pc} = 0.04(1)$ μs^{-1}. The Gaussian component of the relaxation is nearly temperature independent below 100 K, in agreement with Ref. 40, and decreases gradually above 100 K. Figure 10(b) shows the normalized temperature dependence of σ_{pc} for sample A in the transverse-field mode and for sample B in the zero-field mode. Although the starting value of $\sigma_{pc}(0)$ is different for both samples, their normalized temperature dependence is almost identical and not depending on the mode of measurement (transverse field or zero field).

An analysis of the μSR time spectra of $Nd_{1-x}Pr_xBa_2Cu_3O_{7-\delta}$ in the MP35N pressure cell used in the present study with Eq. (1) yields at temperatures below 100 K $\sigma_{pc}(0) = 0.31(1)$ μs^{-1}. The temperature dependence of σ_{pc} was obtained from the corresponding normalized data shown in Fig. 10(b). The temperature-independent exponential component of the muon relaxation rate of the pressure cell with $\lambda_{pc} = 0.04$ μs^{-1} was used.

APPENDIX B: MAGNETIZATION MEASUREMENTS OF PrBa$_2$Cu$_3$O$_{7-\delta}$

In order to detect the presence or absence of a superconducting phase with increasing hydrostatic pressure, magnetization measurements were performed for $PrBa_2Cu_3O_{7-\delta}$ in field-cooled conditions at an applied field of $\mu_0 H = 1$ mT. The diamond anvil type of pressure cell with a volume under pressure $V_P \simeq 0.1$ mm^3 was loaded with a $PrBa_2Cu_3O_{7-\delta}$ sample and a small piece of Pb. The volume of the sample is about half of V_P while the volume of Pb is at least a factor of $f = 5$ smaller than that of the sample. The small piece of Pb inside of V_P serves as a pressure manometer while another piece of Pb outside of V_P serves as a reference of the Pb superconducting transition temperature T_c^{Pb} at zero pressure. Daphne oil was used as a pressure transmission medium. The results of these measurements for $P = 0$, 1.35, and 2.3 GPa are shown in Fig. 11(a). The magnetization of the pressure cell was measured in a separate experiment and subtracted. No diamagnetism can be detected within precision of the experiment. Systematic and statistical errors of the measured magnetic moments are of the order of 0.2 nA m^2. Figure 11(b) shows the magnetization measurements of the superconducting transitions of lead T_c^{Pb}s inside and outside of
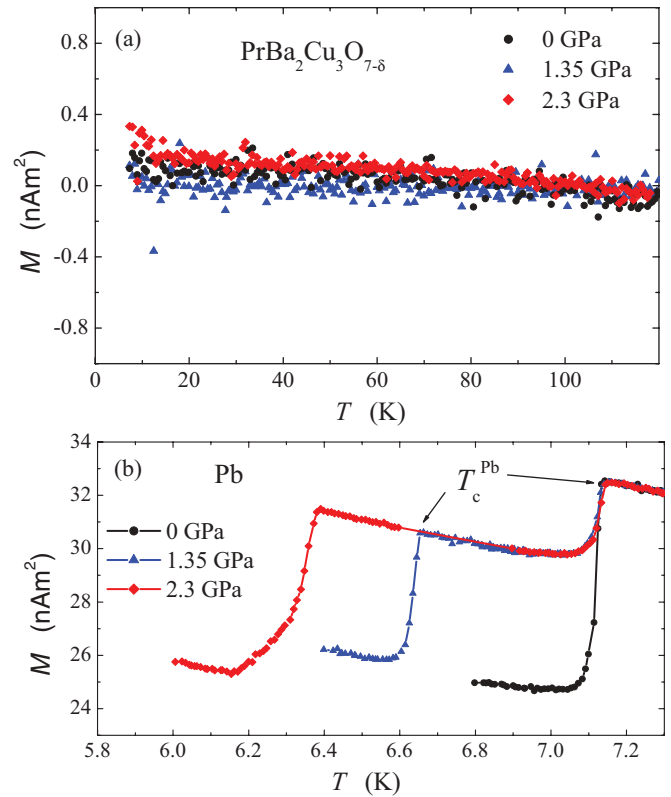

FIG. 11. (Color online) (a) Field-cooled magnetization measurements of 0.5(2) mg of $PrBa_2Cu_3O_{7-\delta}$ in an applied field of $\mu_0 H = 1$ mT. The background magnetization of the pressure cell is subtracted. (b) Magnetic moment of the pressure cell and the sample in a temperature range below 7.3 K showing the superconducting transition temperature of lead pieces inside and outside of the pressure cell (indicated by arrows for $P = 1.35$ GPa). The pressure cell background signal is not subtracted.

V_P at $P = 0$, 1.35, and 2.3 GPa. At $P = 2.3$ GPa the transition of Pb is broadened due to a pressure inhomogeneity. The magnetic moment is also slightly increased, since lead flows around the nonsuperconducting grains of the sample and increases its effective volume. The difference of these transition temperatures allows us to determine the applied pressure, while the drop of the magnetic moment $\delta M^{Pb} \simeq -5$ nA m^2 below T_c^{Pb} shows the sensitivity of the measurement. Namely, for a 100% superconducting $PrBa_2Cu_3O_{7-\delta}$ sample one expects a drop of the magnetic moment $\Delta M^{Pr} = f \times \delta M^{Pb} = -25$ nA m^2 below the respective T_c^{Pr}. Since we can clearly exclude the presence of a diamagnetic moment greater than $\delta m = -0.2$ nA m^2 a possible superconducting volume fraction is smaller than $\delta m / \Delta M^{Pr} = 0.2/25 = 0.008 \simeq 1\%$. Thus, we do not detect the presence of a superconducting phase in our $PrBa_2Cu_3O_{7-\delta}$ samples up to 2.3 GPa.

*alexander.m@physik.uzh.ch

[1]M. B. Maple, Y. Dalichaolkh, J. M. Ferreira, R. R. Hake, B. W. Lee, J. J. Neumeier, M. S. Torikachvili, K. N. Yang, H. Zhou, R. P. Gaurtin, and M. V. Kuric, Physica B **148**, 155 (1987).

[2]Y. Xu and W. Guan, Appl. Phys. Lett. **53**, 334 (1988).

[3]C. R. Fincher Jr. and G. B. Blanchet, Phys. Rev. Lett. **67**, 2902 (1991).

[4]J. G. Lin, C. Y. Huang, Y. Y. Xue, C. W. Chu, X. W. Cao, and J. C. Ho, Phys. Rev. B **51**, 12900 (1995).

[5]There are no reports for $Pm_{1-x}Pr_xBa_2Cu_3O_7$ since it is highly radioactive.

[6] L. Soderholm, K. Zhang, D. G. Hinks, M. A. Beno, J. D. Jorgensen, C. U. Segre, and Ivan K. Schuller, Nature (London) **328**, 604 (1987).

[7] H. B. Radousky, J. Mater. Res. **7**, 1917 (1992).

[8] M. Akhavan, Physica B **321**, 265 (2002).

[9] G. Nieva, S. Ghamaty, B. W. Lee, M. B. Maple, and I. K. Schuller, Phys. Rev. B **44**, 6999 (1991).

[10] Y. Xu and W. Guan, Phys. Rev. B **45**, 3176(R) (1992); W. Guan, Y. Xu, S. R. Sheen, Y. C. Chen, J. Y. T. Wei, H. F. Lai, M. K. Wu, and J. C. Ho, *ibid.* **49**, 15993 (1994); W. Y. Guan, Y. C. Chen, J. Y. T. Wei, Y. H. Xu, and M. K. Wu, Physica C **209**, 19 (1993).

[11] A. Kebede, C. S. Jee, J. Schwegler, J. E. Crow, T. Mihalisin, G. H. Myer, R. E. Salomon, P. Schlottmann, M. V. Kuric, S. H. Bloom, and R. P. Guertin, Phys. Rev. B **40**, 4453 (1989).

[12] L. Soderholm, C.-K. Loong, G. L. Goodman, and B. D. Dabrowski, Phys. Rev. B **43**, 7923 (1991).

[13] H.-D. Jostarndt, U. Walter, J. Harnischmacher, J. Kalenborn, A. Severing, and E. Holland-Moritz, Phys. Rev. B **46**, 14872 (1992).

[14] Z. Klencsár, E. Kuzmann, A. Vértes, P. C. M. Gubbens, A. M. van der Kraan, M. Bódogh, and I. Kotsis, Physica C **329**, 1 (2000).

[15] R. Khasanov, A. Shengelaya, D. Di Castro, E. Morenzoni, A. Maisuradze, I. M. Savić, K. Conder, E. Pomjakushina, A. Bussmann-Holder, and H. Keller, Phys. Rev. Lett. **101**, 077001 (2008).

[16] S. K. Agarwal and A. V. Narlikar, Prog. Cryst. Growth Charact. **28**, 219 (1994).

[17] *Superconductivity in Complex Systems*, edited by K. A. Müller and A. Bussmann-Holder, Structure and Bonding 114 (Springer-Verlag, Berlin, 2005), pp. 114–143.

[18] Patrick A. Lee, Naoto Nagaosa, and Xiao-Gang Wen, Rev. Mod. Phys. **78**, 17 (2006).

[19] R. Fehrenbacher and T. M. Rice, Phys. Rev. Lett. **70**, 3471 (1993).

[20] A. I. Liechtenstein and I. I. Mazin, Phys. Rev. Lett. **74**, 1000 (1995).

[21] I. I. Mazin and A. I. Liechtenstein, Phys. Rev. B **57**, 150 (1998).

[22] H. A. Blackstead, J. D. Dow, D. B. Chrisey, J. S. Horwitz, M. A. Black, P. J. McGinn, A. E. Klunzinger, and D. B. Pulling, Phys. Rev. B **54**, 6122 (1996).

[23] Z. Zou, K. Oka, T. Ito, and Y. Nishihara, Jpn. J. Appl. Phys., Part 2 **36**, L18 (1997); Z. Zou, J. Ye, K. Oka, and Y. Nishihara, Phys. Rev. Lett. **80**, 1074 (1998).

[24] J. Ye, Z. Zou, A. Matsushita, K. Oka, Y. Nishihara, and T. Matsumoto, Phys. Rev. B **58**, 619(R) (1998).

[25] I. I. Mazin, Phys. Rev. B **60**, 92 (1999).

[26] J. J. Neumeier, M. B. Maple, and M. S. Torikachvili, Physica C **156**, 574 (1988).

[27] J. G. Lin, C. Y. Huang, and J. C. Ho, Physica C **340**, 79 (2000).

[28] J. G. Lin, C. Y. Huang, Y. Y. Xue, C. W. Chu, X. L. Cheng, and J. C. Ho, Phys. Rev. B **53**, 11855 (1996).

[29] J. G. Lin, Y. Y. Xue, C. W. Chu, X. W. Cao, and J. C. Ho, J. Appl. Phys. **73**, 5871 (1993).

[30] For a given x the chemical pressure can be increased by reducing the ionic size of the isovalent rare-earth element $R^{3+} = La^{3+}, Nd^{3+}, Sm^{3+}, \ldots, Yb^{3+}, Lu^{3+}$.

[31] For a small concentration x ($0 < x \ll x_{cr}$) a positive PE on T_c has been observed that is presumably caused by a transfer of charge from the chain to the plane sites, also observed in $YBa_2Cu_3O_{7-\delta}$ (Refs. 52–54).

[32] C. Jee, A. Kebede, T. Yuen, S. H. Bloom, M. V. Kuric, J. E. Crow, R. P. Guertin, T. Mihalisin, G. H. Myer, and P. Schlottmann, J. Magn. Magn. Mater. **76 & 77**, 617 (1988).

[33] S. S. Weng, I. P. Hong, C. F. Chang, H. L. Tsay, S. Chatterjee, H. D. Yang, and J.-Y. Lin, Phys. Rev. B **59**, 11205 (1999).

[34] S. J. S. Lister, A. T. Boothroyd, N. H. Andersen, A. A. Zhokhov, A. N. Christensen, and Th. Wolf, Physica C **317-318**, 572 (1999).

[35] S. J. Blundell, Contemp. Phys. **40**, 175 (1999).

[36] A. Yaouanc and P. Dalmas de Reotier, *Muon Spin Rotation, Relaxation, and Resonance: Applications to Condensed Matter*, International Series of Monographs on Physics 147 (Oxford University Press, Oxford, 2011).

[37] J. Rodríguez-Carvajal, Physica B **192**, 55 (1993).

[38] S. R. Ghorbani, M. Andersson, and Ö. Rapp, Phys. Rev. B **69**, 014503 (2004).

[39] J. Kamarád, Z. Machátová, and Z. Arnold, Rev. Sci. Inst. **75**, 5022 (2004).

[40] D. Andreica, *Magnetic Phase Diagram in Some Kondo-Lattice Compounds: Microscopic and Macroscopic Studies* (ETH, Zürich, 2001).

[41] A. Maisuradze, A. Shengelaya, A. Amato, E. Pomjakushina, and H. Keller, Phys. Rev. B **84**, 184523 (2011).

[42] D. W. Cooke, M. S. Jahan, R. S. Kwok, R. L. Lichti, T. R. Adams, C. Boekema, W. K. Dawson, A. Kebede, J. Schwegler, J. E. Crow, and T. Mihalisin, Hyperfine Interact. **63**, 213 (1990); D. W. Cooke, R. S. Kwok, R. L. Lichti, T. R. Adams, C. Boekema, W. K. Dawson, A. Kebede, J. Schwegler, J. E. Crow, and T. Mihalisin, Phys. Rev. B **41**, 4801(R) (1990).

[43] T. M. Riseman, J. H. Brewer, E. J. Ansaldo, P. M. Grant, M. E. Lopez-Morales, and B. M. Sternlieb, Hyperfine Interact. **63**, 249 (1990).

[44] S. J. Blundell, T. Lancaster, F. L. Pratt, P. J. Baker, W. Hayes, J.-P. Ansermet, and A. Comment, Phys. Rev. B **81**, 092407 (2010).

[45] H. H. Aslanian, M. Tun, M. M. Abdelrazek, S. X. Cavanaugh, and C. Boekema, Physica C **364-365**, 582 (2001).

[46] W-H. Li, J. W. Lynn, S. Skanthakumar, T. W. Clinton, A. Kebede, C.-S. Jee, J. E. Crow, and T. Mihalisin, Phys. Rev. B **40**, 5300 (1989).

[47] A. T. Boothroyd, A. Longmore, N. H. Andersen, E. Brecht, and Th. Wolf, Phys. Rev. Lett. **78**, 130 (1997).

[48] J. P. Hill, D. F. McMorrow, A. T. Boothroyd, A. Stunault, C. Vettier, L. E. Berman, M. v. Zimmermann, and Th. Wolf, Phys. Rev. B **61**, 1251 (2000).

[49] J. P. Hill, A. T. Boothroyd, N. H. Andersen, E. Brecht, and Th. Wolf, Phys. Rev. B **58**, 11211 (1998).

[50] J. M. Tranquada, D. E. Cox, W. Kunnmann, H. Moudden, G. Shirane, M. Suenaga, P. Zolliker, D. Vaknin, S. K. Sinha, M. S. Alvarez, A. J. Jacobson, and D. C. Johnston, Phys. Rev. Lett. **60**, 156 (1988).

[51] J. Kikuchi, I. Terasaki, T. Machi, S. Tajima, N. Koshizuka, N. Seiji, S. Adachi, K. Tanabe, C. Murayama, and N. Môri, Phys. Rev. B **59**, 3385 (1999).

[52] W. L. Hults, J. C. Cooley, E. J. Peterson, J. L. Smith, H. A. Blackstead, and J. D. Dow, Int. J. Mod. Phys. **12**, 3278 (1998).

[53] J. C. Cooley, W. L. Hults, E. J. Peterson, and J. L. Smith, Int. J. Mod. Phys. **12**, 3254 (1998).

[54] C. C. Almasan, S. H. Han, B. W. Lee, L. M. Paulius, M. B. Maple, B. W. Veal, J. W. Downey, A. P. Paulikas, Z. Fisk, and J. E. Schirber, Phys. Rev. Lett. **69**, 680 (1992).

[55] R. P. Gupta and M. Gupta, Phys. Rev. B **51**, 11760 (1995).

[56] X. J. Chen, H. Q. Lin, and C. D. Gong, Phys. Rev. Lett. **85**, 2180 (2000).